Relaxation times, rheology, and finite size effects for non-Brownian disks in two dimensions

Peter Olsson*
Department of Physics, Umeå University, 901 87 Umeå, Sweden

(Received 2 December 2021; accepted 1 March 2022; published 16 March 2022)

We carry out overdamped simulations in a simple model of jamming—a collection of bidisperse soft core frictionless disks in two dimensions—with the aim to explore the finite size dependence of different quantities, both the relaxation time obtained from the relaxation of the energy and the pressure equivalent of the shear viscosity. The motivation for the paper is the observation [Nishikawa *et al.*, J. Stat. Phys. **182**, 37 (2021)] that there are finite size effects in the relaxation time, τ, that give problems in the determination of the critical divergence, and the claim that this is due to a finite size dependence, $\tau \sim \ln N$, which makes τ an ill-defined quantity. Beside analyses to determine the relaxation time for the whole system we determine particle relaxation times which allow us to determine both histograms of particle relaxation times and the average particle relaxation times—two quantities that are very useful for the analyses. The starting configurations for the relaxation simulations are of two different kinds—completely random or taken from steady shearing simulations—and we find that the difference between these two cases are bigger than previously noted and that the observed problems in the determination of the critical divergence obtained when starting from random configurations are not present when instead starting the relaxations from shearing configurations. We also argue that the the effect that causes the $\ln N$ dependence is not as problematic as asserted. When it comes to the finite size dependence of the pressure equivalent of the shear viscosity we find that our data don't give support for the claimed strong finite size dependence, but also that the finite size dependence is at odds with what one would normally expect for a system with a diverging correlation length, and that this calls for an alternative understanding of the phenomenon of shear-driven jamming.

DOI: 10.1103/PhysRevE.105.034902

I. INTRODUCTION

The jamming transition is a zero-temperature phase transition from a fluid at low density to a disordered solid at a larger density [1]. Much work on the jamming transition has centered on static packings produced by starting from random configurations and moving the particles to relax the energy related to the particle overlaps and thus generate packings with vanishing overlap [2]. Another path towards jamming is through shearing simulations [3], which are usually done at constant (low) shear rates, and one then finds that the shear viscosity exhibits a critical divergence as the jamming density is approached from below [4,5].

The determination of the critical exponent of this transition—the shear-driven jamming transition—has, however, turned out to be a difficult task, both in experiments and in simulations [4–12], and that is for two reasons: first, because of the difficulty to get reliable values of the viscosity, $\eta(\phi)$ at densities ϕ close to jamming and, second, because the jamming density, ϕ_J, is not known and the value of the exponent depends sensitively on ϕ_J. A way to circumvent this second difficulty and determine a critical divergence—albeit a different one—is by instead examining the dependence on the average number of contacts, z, which is advantageous since its value at jamming is known to be $z_c = 2d$. This kind of approach was pioneered by Lerner *et al.* [13] in a work where they determined the pressure of sheared hard disks below ϕ_J with an innovative simulation method. They were then able to determine a critical exponent from the slope of $\eta_p \equiv p/\dot{\gamma}$ where p is pressure and $\dot{\gamma}$ is the shear strain rate (η_p is just p in their notation) vs $\delta z \equiv z_c - z$. By furthermore examining the vibrational modes it was clear that there is a unique lowest vibrational mode with frequency $\omega_{\min}$, which is directly related to η_p. It turns out that this mode spans the whole system and is closely related to the shearing.

A limitation of the method of Ref. [13] is that a matrix equation has to be solved every time the contact network is changing, which is something that happens more frequently as the simulations are performed closer to jamming. A different way to get similar nonoverlapping configurations is by doing two-step simulations [14]: first, running ordinary shearing simulations of soft particles and, second, performing relaxation simulations from such starting configurations. For each such simulation the relaxation time was determined from the exponential decay of energy (or pressure, as in Ref. [14]) to the nonoverlapping limit. This relaxation time τ, determined in overdamped dynamics, turns out to be directly related to $1/\omega_{\min}^2$ in a Newtonian dynamics [13,14]. These quantities are also found to behave the same as η_p [13–15]. To be clear,

*Peter.Olsson@tp.umu.se

the determination of the relaxation time τ also suffers from problems at the approach to ϕ_J, as the simulation times are proportional to the relaxation times, which grow rapidly as jamming is approached.

Another way to determine the critical behavior is through a scaling analysis of η_p that generalizes the behavior $\eta_p \sim (\phi_J - \phi)^{-\beta}$, valid for hard disks—or, equivalently, for soft disks in the limit $\dot{\gamma} \to 0$—to finite shear rates [4,16]. There do, however, seem to be weaknesses with all methods, and for these scaling analyses it is the presence of large corrections to scaling that badly complicates the analyses. A related method that handles the correction to scaling term differently was used in [17].

The first two of these methods were used in the recent, unexpected, finding of different critical behaviors in two and three dimensions [18]. This result has, however, been questioned since it is difficult to reconcile with other results that suggest that the upper critical dimension should be equal to two [19,20]—implying that the critical exponents should be the same for all $D \geqslant 2$, but possibly complicated by log corrections for $D = 2$.

With the above two methods in different ways determining the divergence by making use of shearing simulations, the report of similar results when instead relaxing from random configurations [21] was quite unexpected as it suggested that the shearing is not a prerequisite for getting a configuration with a well-defined relaxation time. The picture was, however, complicated even more when another paper from the same group [22] argued for problems with the analyses due to the neglect of a finite size effect. The main complaint was that there is a finite size dependence in the relaxation time, $\tau \sim \ln N$, which makes τ an ill-defined quantity which cannot be used for determining the critical behavior. This finite size effect—which we here call the NIB effect for Nishikawa, Ikeda, and Berthier—is that systems with linear size L bigger than a certain characteristic length, $L > \xi_{\text{force}}$ (see below or in Ref. [22] for the definition of ξ_{force}) split into islands that relax independently. The final relaxation of the total energy is then governed by the island with the largest relaxation time and the fact that a bigger system tends to have a bigger "largest relaxation time" leads to the system size dependence $\tau \sim \ln N$ [22].

Of relevance for the determination of the critical behavior from a scaling analysis of η_p, is a further claim in Ref. [22] that η_p is plagued by severe finite size effects and that only values of η_p for systems with $L > \xi_{\text{force}}$, are to be trusted. Since this length is a rapidly growing function of ϕ, the claim casts doubts on all attempts made hitherto to determine the critical divergence from η_p, as well as the feasibility of such attempts for the future.

The present paper is a critical reexamination of Ref. [22] to see to what extent the conclusions presented there hold for a closer analysis. The conclusions in Ref. [22] of relevance for the present work are (1) that the relaxation time is ill-defined and cannot be used for studying the transition and (2) that the viscosity obtained from accessible system sizes are not useful since they suffer from severe finite size effects. We find these conclusions to be unnecessarily pessimistic.

Our study is on simulations using two different protocols: "shearing," which means that configurations created during steady shearing simulations at different constant shear rates are used as starting points in relaxation simulations, performed with $\dot{\gamma} = 0$ [14], and "random," which means that the initial configurations are created by positioning the particles in random [21,22]. Our findings may be summarized as follows: (1) There are big differences between the results from the random case and the results from the shearing case, shown by the finite size dependence of τ being much more pronounced in the random case. This finite size effect is, however, often unrelated to the NIB effect mentioned above. (2) We determine the relaxation time of the individual particles, τ_p, and use them first to make histograms $H(\tau_p)$ which allow for direct studies of the NIB effect and second to determine the average relaxation time, $\langle \tau_p \rangle$. It turns out that this is a quantity with a well-defined thermodynamic limit which thus opens up for a determination of the critical behavior. (3) In our search for the origin of this additional finite size dependence we then turn to the density fluctuations that are present in randomly generated configurations before the relaxations, and we find that the finite size dependence in these fluctuations, to some extent, survives into the relaxed configurations. We argue that this is at the root of the finite size dependence in τ as well as in other quantities. (4) A finite size dependence of τ was found in Ref. [22] to invalidate the attempts to determine the critical divergence. We confirm the same kind of effect also at higher densities and larger system sizes for the random case but find that it is not present in the shearing case, and argue that it is the large density fluctuations that lead to relaxed systems that have problematic properties as evidenced in several different quantities. (5) We also examine the relation between island size and relaxation time valid in the NIB region where the system splits into different islands and find a direct proportionality between these quantities. The same kind of relation is also obtained analytically for a one-dimensional model. Another simple analytical argument gives a relation between island size and density and suggests $\tau \sim (-\delta\phi)^{-2}$, where $\delta\phi = \phi - \phi_J$, in good agreement with the behavior of $\langle \tau_p \rangle$ well below jamming. (6) We then turn to determinations of the correlation C_{force} and the associated length ξ_{force} introduced in Ref. [22] and find that even though the height of the maxima of C_{force} differ by more than an order of magnitude for our two different protocols, the length ξ_{force} is about the same. (7) We finally consider finite size effects on η_p and find that the onset of the finite size effect takes place at the same system size for different densities in the range $\phi = 0.830$ through 0.838, which is at odds with the general expectation for finite size effects in critical phenomena, and is in contrast to the claim in Ref. [22] of very severe finite size effects in η_p.

The organization of the paper is as follows: In Sec. II we introduce the simulation methods and the measured quantities, in Sec. III we give results for the relaxation simulations, in Sec. IV we present the finite size study of the pressure equivalent of the viscosity, and in Sec. V we summarize the results.

II. MODELS AND MEASURED QUANTITIES

For the simulations we follow O'Hern *et al.* [2] and use a simple model of bidisperse frictionless disks in two

dimensions with equal numbers of particles with two different radii in the ratio 1.4. Length is measured in units of the diameter of the small particles, d_s. We use Lees-Edwards boundary conditions [23] to introduce a time-dependent shear strain $\gamma = t\dot{\gamma}$. With r_{ij} the distance between the centers of two particles and d_{ij} the sum of their radii, the relative overlap is $\delta_{ij} = 1 - r_{ij}/d_{ij}$, and the interaction between overlapping particles is $V(r_{ij}) = \epsilon\delta_{ij}^2/2$; we take $\epsilon = 1$. The force on particle i from particle j is $\mathbf{f}_{ij}^{\rm el} = -\nabla_i V(r_{ij})$, which gives the magnitude $f_{ij}^{\rm el} = \epsilon\delta_{ij}/d_{ij}$. The simulations are performed at zero temperature.

We consider the interaction force $\mathbf{f}_i^{\rm el} = \sum_j \mathbf{f}_{ij}^{\rm el}$ where the sum extends over all particles j in contact with i. The simulations discussed here have been done with the RD_0 (reservoir dissipation) model [24] with the dissipating force $\mathbf{f}_i^{\rm dis} = -k_d\mathbf{v}_i$ where $\mathbf{v}_i \equiv \mathbf{v}_i^{\rm tot} - y_i\dot{\gamma}\hat{x}$ is the nonaffine velocity, i.e., the velocity with respect to a uniformly shearing velocity field, $y_i\dot{\gamma}\hat{x}$. In the overdamped limit the equation of motion is $\mathbf{f}_i^{\rm el} + \mathbf{f}_i^{\rm dis} = 0$, which becomes $\mathbf{v}_i = \mathbf{f}_i^{\rm el}/k_d$. We take $k_d = 1$ and the time unit $\tau_0 = d_s^2 k_d/\epsilon = 1$. The equations of motion were integrated with the Heuns method with time step $\Delta t/\tau_0 = 0.2$. We simulate with $N = 256$ through $1\,048\,576 \approx 10^6$ particles to study finite size effects.

To determine the relaxation time we run simulations as described above at zero temperature and fixed γ which leads to an energy decreasing down towards zero; the simulations are aborted when the energy per particle is $E < 10^{-20}$. The relaxation time is then determined from the exponential decay of the energy per particle by fitting $E(t)$ to

$$E(t) \sim e^{-t/\tau}, \quad E(t) < 10^{-17}. \tag{1}$$

For each parameter set the data are based on four to typically 100 different relaxations, but sometimes up to 1000. The lower number is for some of the simulations for systems with $N \approx 10^6$, where fluctuations are small. The bigger numbers are for the smaller N.

A key observation in Ref. [22] is that different regions of the system may exhibit different decay rates. To study this phenomenon we introduce and examine the relaxation time of the energy for different particles. The elastic energy related to particle i is $E_i = \frac{1}{2}\sum_j \epsilon\delta_{ij}^2/2$, where the sum is over all particles j in contact with i. The relaxation time for particle i, $\tau_p^{(i)}$, is then determined from the final stage of the relaxation of E_i, from configurations stored during the relaxation. These configurations are stored with a time interval Δ, from 100 to 10 000 time units. The smaller Δ are necessary to determine the shorter relaxation times that are present at lower densities.

Using $E_i(t) \sim e^{-t/\tau_p^{(i)}}$ and letting t' be the largest time for which $E_i(t) > 10^{-20}$, the particle relaxation time is determined from

$$\tau_p^{(i)} = \frac{\Delta}{\ln[E_i(t'-\Delta)/E_i(t')]}. \tag{2}$$

From these relaxation times, calculated for all particles, we determine histograms $H(\tau_p)$. There is then always a small fraction of particles with unreasonable relaxation times because of unstable configurations, e.g., because they have only a single contact. These particles are skipped in the final calculation of averages.

For big systems and large relaxation times we have found that one can get artifacts in the determinations of $\tau_p^{(i)}$ due to the finite precision in the double precision numbers used for the positions. This is an effect both of the fact that fewer bits are available for the fraction part when storing larger coordinate values, which leads to a lower precision in the position variables, and the fact that the net force, f_i, is typically a factor of τ (which may be close to a factor 10^5) smaller than the typical interparticle force, f_{ij}, which means that the interparticle forces need to be obtained with high precision. To handle that problem the relaxations for the biggest N at the higher densities were run with a version of the simulation program which uses two variables—for integer part and fraction—to store to position coordinates. The artifacts mentioned above were eliminated in that program version.

To examine the different simulation protocols we study the density fluctuations in both initial and relaxed configurations—for the different cases of random and shearing—and how these fluctuations depend on the size of a circular region R. This is done by measuring $A(R)$, which is the total amount of particle area that is inside a circle of radius R, such that the particles on the boundary contribute with only the fraction of their area which is inside the circle. These areas are measured for a large number of different configurations and center points, and the variance is obtained from

$$\sigma_A^2 = \langle A^2(R)\rangle - \langle A(R)\rangle^2. \tag{3}$$

For initial random configurations and $R \ll L$ the quantity $\sigma_A/\sqrt{N_R}$, where $N_R = (\pi R^2/V)N$ is the average number of particles inside R, approaches a constant, as discussed in Appendix B, and we therefore find it convenient to use that quantity rather than the density fluctuations. The relation to the density fluctuations, determined in the context of hyperuniformity [25], is $\mathrm{var}(\phi_R) = \sigma_A^2/(N_R\langle a\rangle\pi R^2)$, where $\langle a\rangle = \pi(d_s^2 + d_b^2)/8$ (d_b is the diameter of the big disk) is the average particle area.

We also determine the correlation function $C_{\rm force}$ [22] which measures to what extent the net particle forces in the relaxed configurations are correlated [26],

$$C_{\rm force}(r) = \frac{\left\langle \frac{1}{N}\sum_{i<j} \mathbf{f}_i\cdot\mathbf{f}_j\delta(r-r_{ij})\right\rangle}{\left\langle \frac{1}{N}\sum_i \mathbf{f}_i\cdot\mathbf{f}_i\right\rangle}. \tag{4}$$

III. RESULTS

A. Comparison of random and shearing

Figure 1 shows the relaxation times obtained at different $\phi = 0.800$ through 0.838 and for a wide range of number of particles, N. Figure 1(a) shows results after relaxing random configurations, whereas Fig. 1(b) is after relaxing from shearing configurations. For the shearing configurations there are data for initial shear strain rates $\dot{\gamma} = 10^{-7}$ and 10^{-6}, connected by solid and dashed lines, respectively. When there is a shear strain rate dependence the relaxation time decreases with decreasing initial shear strain rate [14].

Figure 1(a) does indeed underscore the message of Ref. [22] of significant finite size effects in τ. From a comparison of the two panels another clear message is the big difference between τ from these different initial conditions.

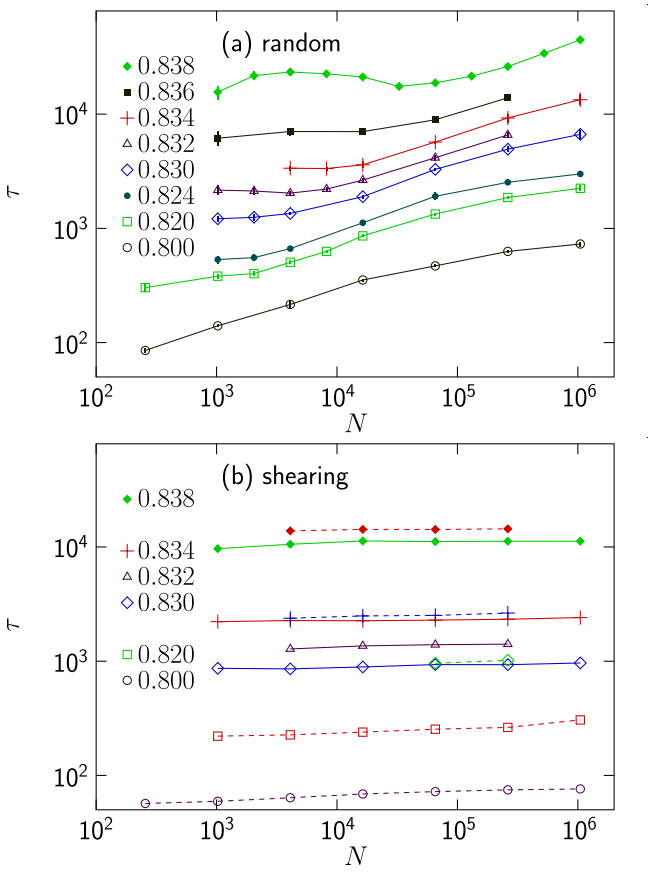

FIG. 1. Finite size dependence of the relaxation time. The figures show the relaxation time from the exponential decay of the energy, Eq. (1), vs number of particles for several different densities. Panel (a) is the behavior when starting from random configurations, whereas panel (b) is the behavior when starting from configurations at steady shearing. The two data sets in panel (b) have been obtained when starting from configurations obtained with two different shear rates. Dashed lines connect data obtained starting from configurations generated with shear rate $\dot{\gamma} = 10^{-6}$; solid lines connect data for $\dot{\gamma} = 10^{-7}$. Note that the finite size dependence is considerably more pronounced when starting from random configurations. There are error bars in the figure, but they are mostly not visible since they are typically smaller than the sizes of the symbols.

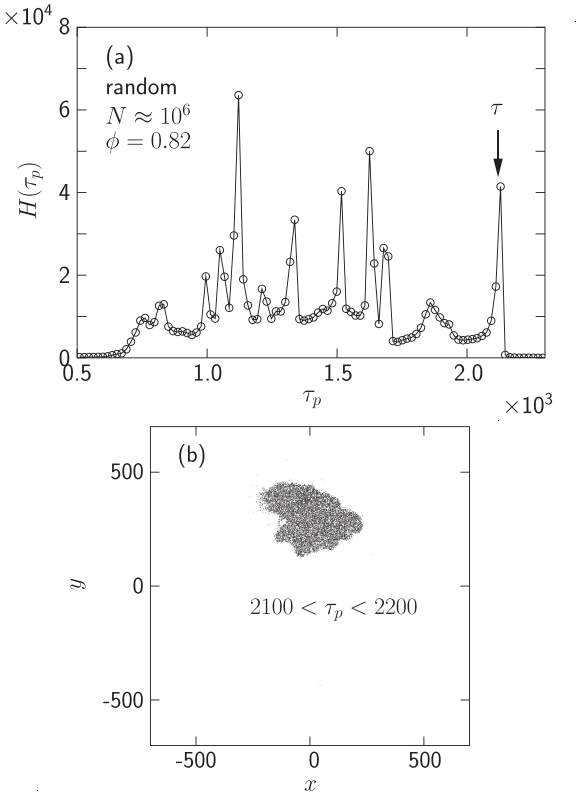

FIG. 2. Histogram of particle relaxation times, τ_p, produced by starting from a single random configuration at $\phi = 0.820$ for $N \approx 10^6$ particles. Panel (a) gives clear evidence for the system splitting up in different parts with different relaxation times. The arrow, which is τ from the decay of the total energy, illustrates that it is the slowest relaxation time that dominates this decay. As argued in Ref. [22] this is at the origin of the $\ln N$ dependence of τ, here coined the NIB effect. Panel (b) shows the positions of the particles in the uppermost peak, which makes clear that that they indeed do belong to a localized island.

The correlation times obtained by relaxing random configurations are consistently larger, and they also show much more pronounced finite size effects.

The explanation in Ref. [22] of the finite size effect is that the increase of τ starts when the system is "large enough to exhibit multiple correlated islands where the relaxation dynamics can take place independently." When that is the case it is the island with the biggest relaxation time that will dominate the long-time behavior and since a bigger system will have a larger number of different such islands it will be expected to have a larger maximum relaxation time which, after a closer analysis, should be $\tau \sim \ln N$ [22].

Though the explanation of this finite size effect—we call it the NIB effect from the authors' names—appears to be correct, we will argue that it cannot be the full story. For more thorough investigations we determine the particle relaxation times τ_p, as described in Eq. (2) and construct histograms $H(\tau_p)$. The NIB effect is illustrated with the histogram in Fig. 2(a) for a single relaxation of a system with $N = 2^{20} \approx 10^6$ particles at $\phi = 0.820$. The peaks at different τ_p are related to islands with different local relaxation times. The value of τ from the energy relaxation, $E \sim e^{-t/\tau}$, shown by the arrow, is close to the peak at the highest τ_p, which is consistent with the expectation that it is the slowest particles that dominate the long time relaxation. Checking a large number of cases we have found that the particles in the uppermost peak of the histogram always make up a localized island. This is illustrated in Fig. 2(b) which shows the positions of the particles with $2100 < \tau_p < 2200$, i.e., the particles from the uppermost peak in Fig. 2(a).

It is however clear that this is not the full explanation of the finite size effects in Fig. 1. That figure shows that $\tau(N)$ is a monotonously increasing function of N for $\phi = 0.820$, and in the log-log plot the slope is actually the biggest around $N \approx 10^4$. Still, the histogram $H(\tau_p)$ from a single relaxation with $N = 16\,384$ in Fig. 3(a) gives evidence for only a single peak, and the same is true for all our 16 examined realizations generated with the same parameters, $\phi = 0.820$ and $N = 16\,384$. This makes clear that there are also other effects

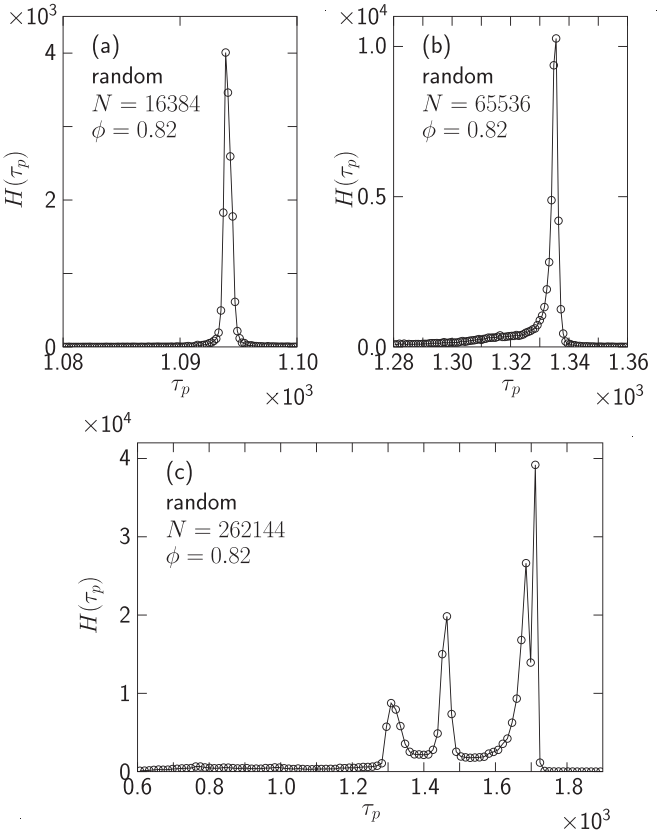

FIG. 3. Histograms of particle relaxation times, τ_p, produced by starting from random configurations at $\phi = 0.820$ for three different system sizes. In panel (a), which is for $N = 16\,384$, all particles have the same relaxation time and there is no NIB effect; nevertheless, this is in a range of N with a strong finite size dependence. The conclusion is that there are also other finite size effects beside the NIB effect. Panel (b) is for an intermediate number of particles, $N = 65\,536$, and we here see a widening of the peak, but also that the histogram extends to lower τ_p, which is a precursor of some more peaks. Panel (c), finally, shows the presence of several peaks for $N = 262\,144$, which is thus the same behavior as in Fig. 2(a).

at play in these systems, besides the NIB effect. The histogram in Fig. 3(b) is for an intermediate number of particles, $N = 65\,536$, where the peak of the histogram is not quite as sharp and one also sees a precursor, below the main peak, of the behavior in Fig. 2(a). Figure 3(c), finally, shows a histogram for the even bigger size, $N = 262\,144$, which shows the presence of several peaks, and is thus very similar to the behavior of Fig. 2(a).

Though the histograms $H(\tau_p)$ open up potentially new possibilities for analyzing the systems, some of the conclusions above may actually be arrived at from the information in Ref. [22]. Since this relates to results throughout the present paper, that discussion is relegated to Appendix A.

To illustrate that there are both similarities and differences between the shearing and the random cases, Fig. 4, which is the same kind of figure as Fig. 2(a), but for the shearing case, shows the histogram $H(\tau_p)$ for the same parameters. There is again a clear signal of the NIB effect, but now as a broad maximum rather than a number of well-separated peaks.

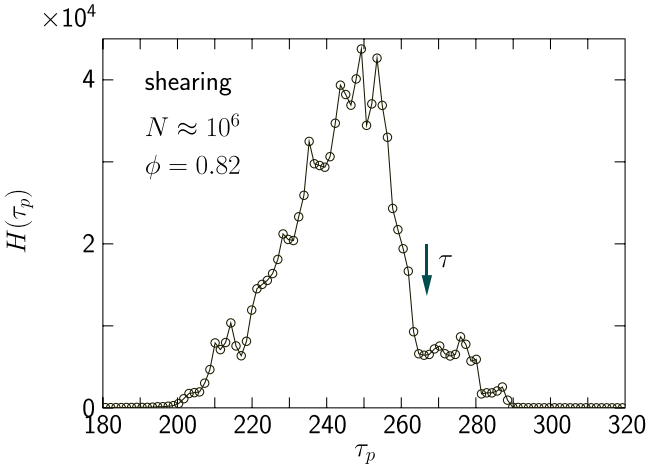

FIG. 4. Histograms of particle relaxation times, τ_p, produced by starting from shearing configurations with $N \approx 10^6$, $\phi = 0.820$, and $\dot{\gamma} = 10^{-6}$.

B. Average particle relaxation time

With access to the particle relaxation times, τ_p, for all individual particles it becomes possible to determine the average τ_p as a different characterization of the system. Since this is an estimate that gives equal weight to all particles and all regions of the system, one would expect this quantity not to be affected by the NIB effect. We use the notation $\langle\tau_p\rangle$ though this quantity (in consistency with τ of [14]) is determined as the geometric average, $\langle x\rangle_{\text{geom}} = \exp(\langle \ln x\rangle)$, rather than an arithmetic average. The different ways to determine the average do not give any noticeable differences for the larger systems, but, as discussed in Ref. [14], the geometric average is a more reasonable quantity for smaller systems.

Figure 5 is $\langle\tau_p\rangle$ and τ vs N for both random and shearing initial configurations. The crosses show $\langle\tau_p\rangle$, whereas the other symbols are τ as in Fig. 1. [To avoid cluttering the figure, Fig. 5(b) shows only the data for the lowest $\dot{\gamma}$ for each ϕ.] In both figures $\langle\tau_p\rangle$ and τ mostly agree very well, and deviations are found only in the lower right corners of low ϕ and big N. The difference between these two quantities is clearly due to the NIB effect and just as mentioned above, $\langle\tau_p\rangle$ for each ϕ appears to approach a constant as $N \to \infty$ whereas τ continues to increase. A dashed line separates the NIB region from the region where the finite size effect is of a different origin.

This finding leads to several conclusions. The first is that $\langle\tau_p\rangle$, in contrast to τ, is a quantity with a well-defined $N \to \infty$ limit, and that it may therefore actually be used to determine the exponent of the critical divergence related to the shear-driven jamming transition.

The second is that it now becomes possible to compare the relaxation time (in terms of $\langle\tau_p\rangle$) for the two cases of random and shearing initial configurations. In the large-N limit it appears that $\langle\tau_p\rangle$ from random configurations is about a factor of six bigger than $\langle\tau_p\rangle$ from shearing configurations.

A third conclusion regards the use of τ to determine the critical behavior from shearing configurations. In Ref. [22] it was argued that τ may not be used to determine the critical behavior for the jamming transition since it has no $N \to \infty$

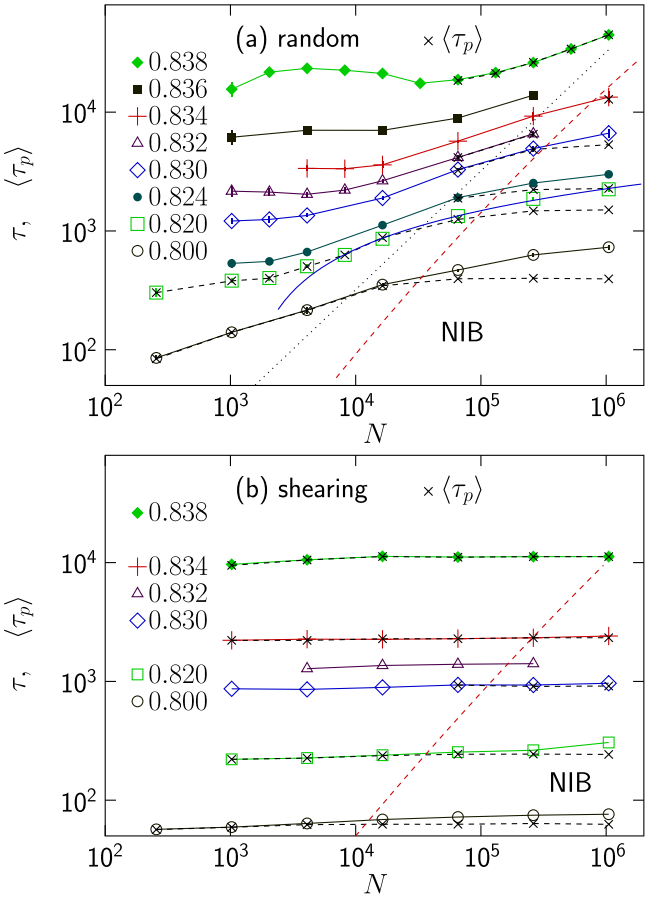

FIG. 5. Finite size dependence of both the relaxation time, shown by different symbols for different ϕ, and the average particle relaxation time, $\langle\tau_p\rangle$, shown by x's. Just as in Fig. 1 panel (a) is from random configurations, whereas panel (b) is from shearing configurations. In each figure the dashed line is the approximate boundary of the NIB region, which is in the lower right part of the figures. In turns out that $\langle\tau_p\rangle$ reaches finite limits for sufficiently large N, which is in contrast to τ, which keeps increasing with increasing N. In both panels the region where τ and $\langle\tau_p\rangle$ differ is the NIB region; the boundary is indicated by the straight dashed line. The solid line in panel (a) through the data for $\phi = 0.820$ (squares) shows that the data are well fitted to an $\ln N$ dependence even outside the NIB region. [The dotted line in panel (a) is the relation between $\tau_{\rm is}$ and $N_{\rm is}$ from Fig. 12.]

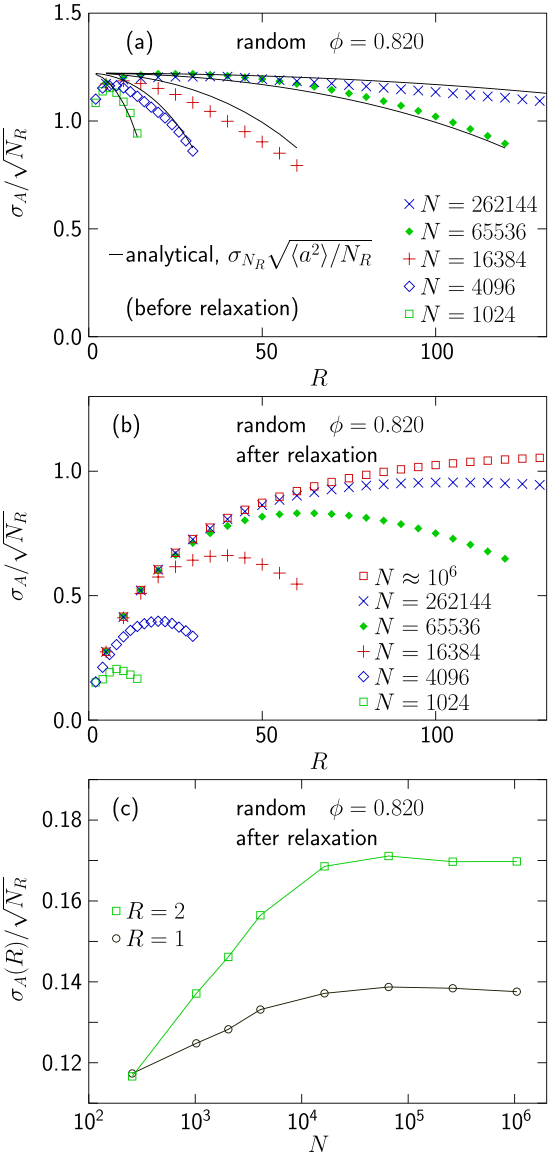

FIG. 6. Density fluctuations for the random case at $\phi = 0.820$ as measured by $\sigma_A/\sqrt{N_R}$. Panel (a) shows this quantity for initial configurations where the behavior is close to $\sigma_{A_c}/\sqrt{N_R}$, given by Eq. (5) and shown by solid lines. Panel (b), which is the same quantity after relaxation, shows that the finite size effects in the initial configurations to a large extent are present also in the relaxed configurations. Panel (c) is the N dependence of $\sigma_A(R)$ for $R = 1$, 2. We see increases in $\sigma_A(r)$ up to $N \approx 65\,536$ where the behavior approaches a constant value, and note that this is similar to the behavior of $\langle\tau_p\rangle$ at $\phi = 0.820$ in Fig. 5(a).

limit. As argued above, $\langle\tau_p\rangle$ may instead be used for this purpose, but since the determination of $\langle\tau_p\rangle$ is considerably more involved than the determination of τ it is interesting to note that τ actually may be used for the parameter values where it may be considered a reliable estimate of $\langle\tau_p\rangle$, which happens to be the case for most of the points in Fig. 5(b) at the higher densities. This also applies to the analyses in Ref. [14] which were done with data for higher densities, $\phi \geqslant 0.838$, only. (For comparisons with some of the figures in Ref. [14] it should be noted that that paper shows τ vs δz, whereas the figures in Ref. [22] and in Sec. III D, below, instead have $\delta z/2d$ on the x axis. There is also a factor of two in difference in τ since it is there determined from the the decay of pressure which depends on the overlap through $p \sim \delta$, whereas τ is here determined from the energy, which is $\sim\delta^2$.)

A consequence of the NIB effect is the behavior $\tau \sim \ln N$, but this kind of behavior of $\tau(N)$ for $\phi = 0.820$ is—quite surprisingly—seen all the way down to $N = 8192$, which is quite far below the NIB region. This is the solid curve in Fig. 5(a). Though we cannot offer any real explanation, we will return to this finding in conjunction with Fig. 6(c) below.

The finding of larger relaxation times from random configurations than from shearing configurations leads to questions about the origin of this difference in $\langle\tau_p\rangle$. It then seems that the lower relaxation time is related to the larger δz and thereby

a lower contact number, which in turn is a sign of a better relaxation. We thus believe that it is the difference in the starting configurations—on the one hand random configurations with huge density fluctuations and on the other configurations with a long smoothing prehistory—that has enormous consequences for the final configurations. Further evidence for this difference is given in the next section.

C. Density fluctuations

We argued above that there is another finite size effect in the random case beside the NIB effect, and we now turn to an attempt to understand its origin through an examination of the size dependence of the density fluctuations. We first examine the density fluctuations in random initial configurations—the configurations before the relaxation step—and show that they may be understood from elementary statistics. We then show that these differences to some extent survive also to the relaxed configurations.

The basic mechanism follows from a consideration of N_R, which is the number of randomly positioned particles that have their centers within a circle of radius R, which is a fraction $f = \pi R^2/V$ of the total volume. This number is trivially on the average $\langle N_R\rangle = fN$, and from the properties of the binomial distribution it follows that the variance of the same quantity is $\sigma^2_{N_R} = f(1-f)N$. Taken together (and simplifying the notation with $\langle N_R\rangle \to N_R$) this becomes

$$\frac{\sigma^2_{N_R}}{N_R} = (1-f).$$

We note that this expression is a constant in the large-N limit but decreases $\propto R^2/N$ for finite N. This is thus the origin of the N dependence in $\sigma_A/\sqrt{N_R}$.

For analyzing our packings without overlaps we have found it convenient to measure $A(R)$, and the related σ^2_A, from Eq. (3). The area $A(R)$ is the total particle area inside a circle of radius R, such that the particles at the boundary contribute with a fraction of their total area, according to definition I in Ref. [25]. A similar quantity which is related to σ_{N_R} is obtained by instead considering the area A_c of the particles with their centers within this circle, such that they always contribute with their total area—definition II in Ref. [25]. Compared to $\sigma^2_{N_R}$ the variance of A_c gets an extra contribution from the different particle sizes, and as shown in Appendix B the expression becomes

$$\frac{\sigma^2_{A_c}}{N_R} = \langle a^2\rangle(1-f), \tag{5}$$

where $\langle a^2\rangle$ is the average particle area squared,

Figure 6(a) shows the area fluctuations $\sigma_A/\sqrt{N_R}$ vs R, determined with Eq. (3) from random initial (unrelaxed) configurations for several different N. The lines are for $\sigma_{A_c}/\sqrt{N_R}$ given by Eq. (5). For the smallest R, the data fall below the lines, as discussed in Appendix B, but otherwise the data agree well with the prediction, considering that these are estimates of fluctuations, which are more difficult to determine with high precision than are averages.

These random initial configurations with high energies and big particle overlaps are then relaxed as discussed above, and the area fluctuations from the relaxed configurations are shown in Fig. 6(b). We note that the density fluctuations for small R are reduced the most, but also that the finite size dependence from the initial configurations to some extent survives into the relaxed configurations such that the area fluctuations are smaller in the smaller systems.

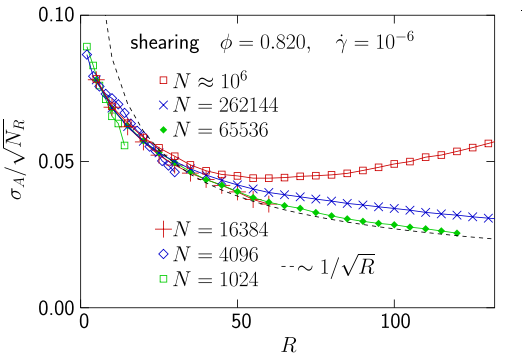

FIG. 7. Density fluctuations for the shearing case at $\phi = 0.820$ as measured by $\sigma_A/\sqrt{N_R}$. This shows that the density fluctuations are always small in configurations obtained with the shearing protocol. For system sizes $N \leqslant 65\,536$, $\sigma_A/\sqrt{N_R}$ is essentially independent of N, but for $N \geqslant 262\,144$—well into the NIB region—this quantity increases with increasing N, presumably because the system there splits into different islands. For comparison the dashed line is $\sim 1/\sqrt{R}$, predicted from hyperuniversality, suggested at ϕ_J.

The density fluctuations for the shearing case are shown in Fig. 7. In this case the fluctuations are considerably smaller—note the different scale. The reason is clearly that the long shearing simulations before the relaxations give homogeneous systems with small density fluctuations even in the unrelaxed systems. For $N \geqslant 262\,144$, in the NIB region, the density fluctuations are however somewhat bigger which is related to the system splitting up into different islands with different local relaxation times and presumably also different densities. We also note that hyperuniformity, suggested to be present in jammed packings at ϕ_J [27] would give $\mathrm{var}(\phi_R) \sim (a + b\ln R)/R^3$ [25] which translates to $\sigma^2_A = (a + b\ln R)/R$. Though our data are far below jamming we find a similar behavior, shown by the dashed line in Fig. 7, which is $\sigma_A \sim 1/\sqrt{R}$, for the data below the NIB region. (We also remark that the density fluctuations, in the shearing case, are essentially the same before and after the relaxation, since there are no big particle displacements during the relaxation.)

Since the density fluctuations are so wildly different for our two different simulation protocols, we believe that they are at the root of the different finite size dependencies of τ in the two panels of Fig. 5, and the effect that gives a large finite size dependence for the random case will now be called the density fluctuation (DF) effect.

A further link between the N dependence of $\langle\tau_p\rangle$ in Fig. 5(a) and the density fluctuations is given by Fig. 6(c) which shows the small R behavior of $\sigma_A(R)$ for $R = 1$, 2. Similarly to the behavior of $\langle\tau_p\rangle$ we find that σ_A increases at low N and approaches constants at large N. The initial increase is $\sigma_A \sim \ln R$, which is similar to the $\ln N$ behavior of $\tau(N)$ at $\phi = 0.820$, which was there found to extend far below the NIB region.

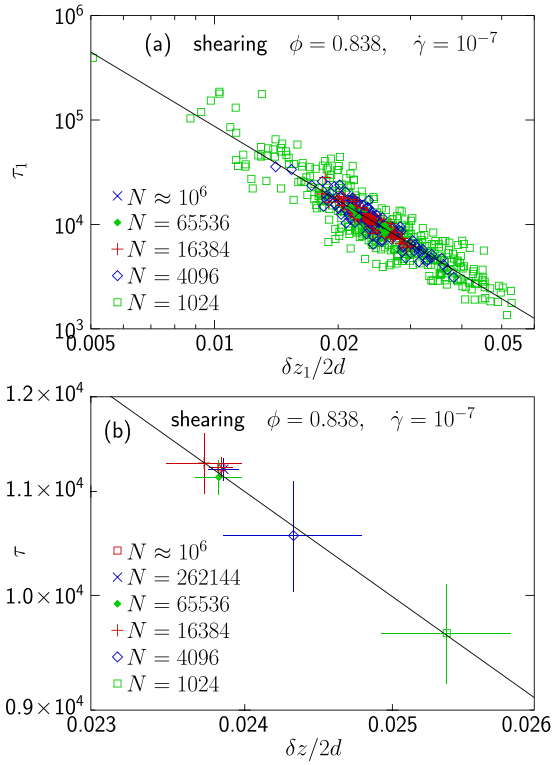

FIG. 8. Relaxation time vs contact deficiency, δ, for the shearing case and different system sizes, $N = 1024$ through $\approx 10^6$. Panel (a) shows individual measurements together with the line with slope $-b$, where $b = 2.36$. Panel (b) shows τ vs δz, which are the geometric averages of the same quantities. This panel shows clearly that the finite size effects are small and unproblematic for the shearing case.

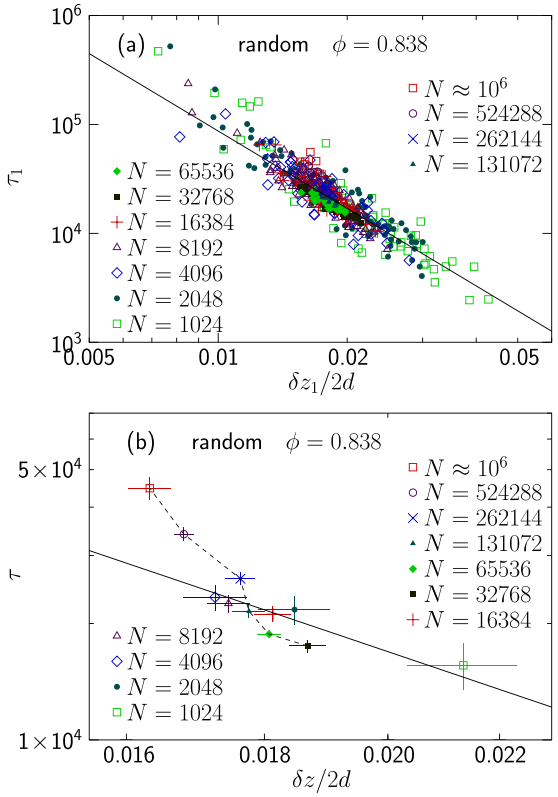

FIG. 9. Relaxation time vs contact deficiency, as $\delta z/2d$, for the random case and different system sizes, $N = 1024$ through $\approx 10^6$. Panel (a) shows individual measurements. Also shown is the line from Fig. 8(a), which is included to illustrate the "universality" suggested in Ref. [21]. To show the results in more detail panel (b) are the geometric averages of τ_1 and δz_1. For sizes up to $N = 16\,384$ seem to agree with the solid line [from Fig. 8(a)], whereas the data for $N \geqslant 32\,768$, connected by the dashed line, deviate clearly.

D. Finite size effects in determinations of the critical exponent

After introducing the particle relaxation times which gives methods for analyzing the NIB effect, and identifying the DF effect, we are now ready to turn to examinations of the critical divergence. From the relation $\tau \sim (\delta z)^{-\beta/u_z}$ it follows that the exponent β/u_z may be determined from the slope of τ vs δz on a double log plot [14], but a test of this approach for the random case in Fig. 1 of Ref. [22] revealed a problematic finite size dependence.

We will now argue that this is a problem for the random case only, and not for the shearing case.

For the shearing case a close look at τ vs N at $\phi = 0.838$ in Fig. 5(b) shows that there is indeed a finite size dependence, and this observation could seem to cast doubt on the use of τ for the determination of the critical divergence. However, as already noted in Ref. [14] it turns out that the finite size dependence of τ is accompanied by a similar finite size dependence of δz, which makes the points $(\tau, \delta z)$ for different N fall on a common curve.

To illustrate this Fig. 8(a) shows τ_1 vs $\delta z_1/2d$ for $\phi = 0.838$ and several different sizes on a double-log scale. The subscript "1" signifies that each point is from a single energy relaxation. The points for the bigger sizes are close together, whereas the points for smaller sizes spread considerably more [14]. The data are suggestive of an algebraic behavior, and a fit gives the line governed by the exponent $-b$, with $b = 2.36$. (For data closer to criticality, i.e., smaller δz and larger τ, this exponent $b \to \beta/u_z \approx 2.7$ [14]; the value $b = 2.36$ is only an effective exponent.) The finite size dependence is too small to be clearly visible in Fig. 8(a), and we therefore calculate τ and δz for the different N as geometric averages of τ_1 and δz_1 and plot τ vs $\delta z/2d$ in Fig. 8(b). It then turns out that the obtained points indeed do fall on the line in the figure, obtained from the fit to the data in Fig. 8(a), and this shows clearly that the observed finite size effect doesn't cause any problems for the determination of the divergence.

For comparison, Fig. 9(a) shows the same kind of data for random starting configurations as in Fig. 8(a), and the first observation is that two data sets are very similar, especially since the solid line, which is taken from Fig. 8(a), fits well to the data. Figure 9(b) which gives the geometric averages, τ and δz, however, shows that there are also some differences. Whereas data for $N \leqslant 16384$ fit nicely to the line, the data for $N \geqslant 524288$ and $\approx 10^6$ are clearly off the line, and it could be that there are deviations from the expected behavior for all the data with $N \geqslant 32\,768$, the points connected by the dashed line. That this is not due to the NIB effect is clear since each of the histograms of τ_p for our six different relaxations with $N \approx 10^6$ and $\phi = 0.838$ has only a single peak.

The finite size dependence in Fig. 9 is the same kind of effect as was first identified in Fig. 1 of Ref. [22] and was

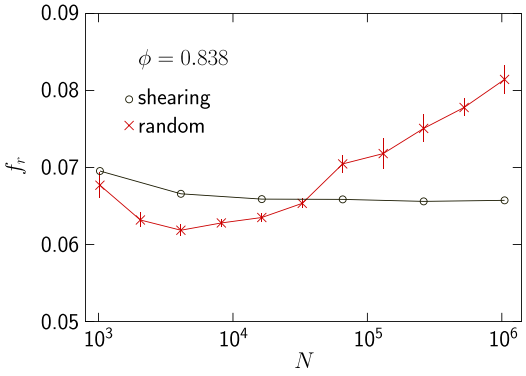

FIG. 10. Fraction of rattlers at $\phi = 0.838$, $N = 1024$ through $N \approx 10^6$ for both the random case and the shearing case. The failure of $f_r(N)$ to saturate for protocol random suggests a problem with this protocol.

there attributed the the NIB effect. From Fig. 5(a) one may, however, again, conclude that this cannot be explained by the NIB effect, since the lowest τ for $N = 262\,144$ in Fig. 1 of Ref. [22] is $\tau \approx 5\times10^3$, whereas the NIB effect is expected to be visible only below $\tau \approx 3\times10^3$. We instead attribute this problematic finite size dependence to the DF effect, which is consistent with this effect being visible for the random case and not for the shearing case.

We have not been able to pinpoint the precise reason for the deviations from the expected algebraic divergence for the random case, but we note that unexpected behaviors are present in many different quantities. One such quantity that behaves strangely in the random case is the fraction of rattlers, shown in Fig. 10 for both the shearing and the random cases. For the shearing case f_r is well behaved and just decreases slowly towards a constant as N increases, but for the random case f_r increases and fails to saturate for our available system sizes. (Note that there is no direct relation between f_r and the contact number z; f_r is related to the number of particles that are eliminated before the calculation of z.) This suggests that the method to relax randomly generated configurations is flawed as it leads to configurations with big density fluctuations and spurious finite size dependencies. Surprising behaviors are indeed also seen in Fig. 5(a) where $\tau(N)$ is nonmonotonic at $\phi = 0.838$, and where precursors of this nonmonotonicity are also found at the lower densities.

The conclusion from this section—which is also one of the main conclusions of the paper—is thus that it is the finite size dependence caused by the DF effect (density fluctuations) that causes problems for the determination of the exponent β/u_z in the random case but that there are no such problems in the shearing case. We stress that the data at high densities investigated here are not affected by the NIB effect, but we also point out that one should watch out for this effect for large systems well below ϕ_J. In the next section we turn to the NIB region and properties of the individual islands.

E. Sizes of islands in the NIB region

In an attempt to get a better understanding of the NIB region—the large-N region where the system splits into different islands—we now examine the relation between relaxation

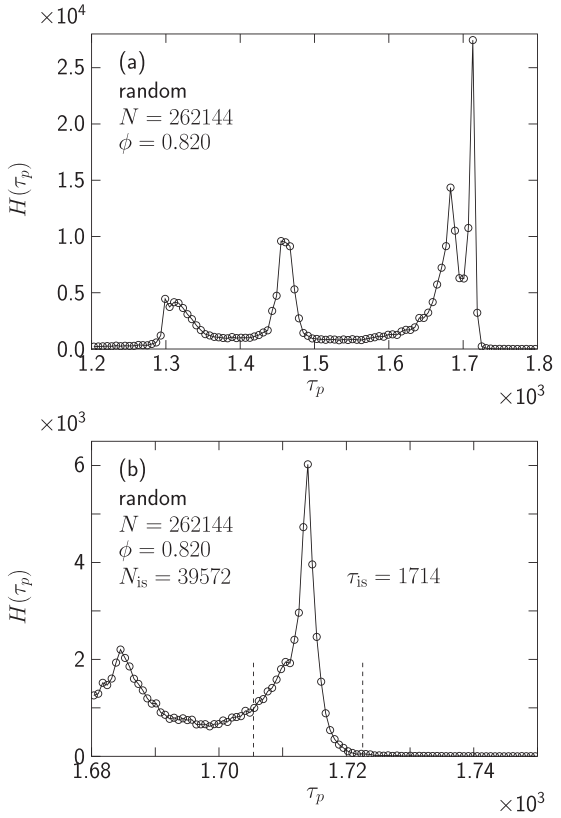

FIG. 11. Determination of $\tau_{\rm is}$ and the size of the island, $N_{\rm is}$, which is the number of particles that belong to the corresponding peak in the histogram. Panel (a) shows the complete histogram, and panel (b) is a zoom in on the uppermost peak. $N_{\rm is}$ is the number of particles with τ_p in the interval $\tau_{\rm is} \pm 0.5\%$.

time and island size. It turns out that there is a direct relation between these quantities such that large correlation times are possible only for big islands. We stress that the results cannot be used to understand the properties outside the NIB region since these systems experience collective relaxations that include all particles in the system, which is a very different process from relaxations of isolated islands.

The determination of the key quantities—the number of particles in an island $N_{\rm is}$ and its relaxation time $\tau_{\rm is}$—is illustrated in Fig. 11, where Fig. 11(a) shows the complete histogram $H(\tau_p)$ and Fig. 11(b) zooms in on the uppermost peak. The relaxation time of the corresponding island is read off from the figure, and $N_{\rm is}$, the number of particles in the peak (and thus also in the corresponding island), is determined from the interval with $\pm0.5\%$ around the peak, as illustrated in the figure. For each configuration we here restrict our analyses to the peak with the biggest relaxation time, to get the cleanest possible analysis. For peaks at lower τ_p there is a higher risk that a peak could sometimes be made up of data from two different islands, which would confuse the analysis.

The relation between island size and relaxation time is shown in Fig. 12 for a number of different configurations with $\phi = 0.800$ through 0.830, generated from random configurations. Since the data give evidence for a linear behavior on a double-log plot with slope $\approx$1, this points to a linear relation, and we find $\tau_{\rm is} \approx 0.032 N_{\rm is}$.

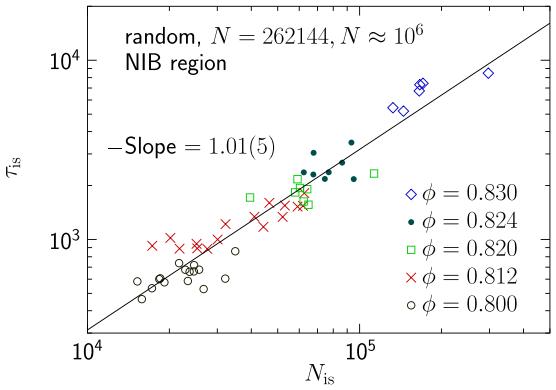

FIG. 12. Relaxation time vs island size in the NIB region determined for the uppermost peaks as shown in Fig. 11(b). The data for $\phi = 0.830$ have been determined with $N \approx 10^6$ particles, whereas the other data are obtained with $N = 262\,144$. The slope 1.01(5) suggests a linear relation which is $\tau_{is} \approx 0.032 N_{is}$.

We now suggest that this linear relation is an effect of the relaxation of a collection of a set of partially overlapping particles. The relation between relaxation time and number of particles in a one-dimensional model with L particles of unit size, initially compressed to have small overlaps, is found in Appendix C to be $\tau \sim L^2$. For the two-dimensional case, with the assumption that it is the lateral size that determines the relaxation time, this translates into $\tau \approx 0.05N$, which is the same conclusion as from Fig. 12, only with a somewhat bigger prefactor. A difference in prefactor is not surprising since the disordered two-dimensional relaxed systems, beside the different dimensionality, are very different from the simple, perfectly ordered one-dimensional model considered in Appendix C.

To make contact with the determination of τ in Fig. 5(a) the relation $\tau_{is} \approx 0.032 N_{is}$ is there shown as a dotted line. For each τ, that line shows the minimum N_{is} of an island with the relaxation time equal to τ. The fact that this line falls slightly to the left of the NIB line is consistent with the fact that a system may have an island of size N_{is} only if it consists of $N > N_{is}$ particles.

It is also possible to construct a simple argument for the relation between density and the average N_{is}, which then also translates into the ϕ dependence of $\langle \tau_p \rangle$. For sufficiently big N we expect a system at a density well below ϕ_J^{rnd} to be too dilute to make up a single well-connected island, and it therefore breaks up into a set of weakly connected (or disjoint) islands with on the average $N_{is}(\phi)$ particles. If one simplifies greatly and considers the islands to be made up of both a dense core with radius R with $\phi \approx \phi_J^{rnd}$ and a thin buffer zone of thickness δ, with no particles, the total area associated with an island with radius R is given by $\pi R^2 + 2\pi R\delta$. By relating this area to the inverse density, and assuming that there is no buffer zone at ϕ_J^{rnd}, the relevant expression becomes

$$\frac{R^2 + 2R\delta}{R^2} = \frac{1/\phi}{1/\phi_J^{rnd}} = \frac{\phi_J^{rnd}}{\phi},$$

and for densities close to ϕ_J^{rnd} we get

$$R \sim \left(\phi_J^{rnd} - \phi\right)^{-1}, \quad N_{is}(\phi) \sim \left(\phi_J^{rnd} - \phi\right)^{-2}.$$

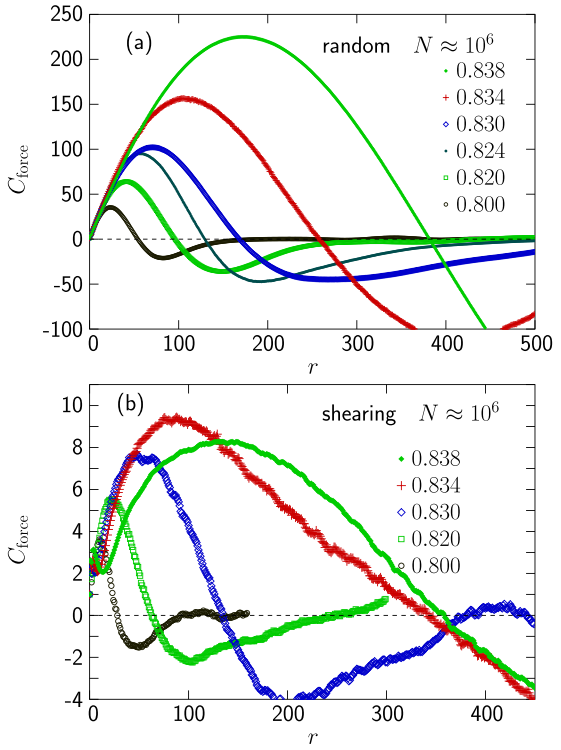

FIG. 13. Force correlation function from Eq. (4) for $N \approx 10^6$ and $\phi = 0.800$ through 0.838. Panel (a) shows $C_{force}(r)$ for the random case, whereas panel (b) is $C_{force}(r)$ for the shearing case. The magnitude of C_{force} is always considerably bigger for the random case than for the shearing case, which is also why the data for the shearing case appear noisier. [In order not to clutter the noisier panel (b), we show only the data for the relevant region in r, somewhat past the crossing that determines ξ_{force}.] For the random case the height of the curves increases with increasing ϕ, whereas for the shearing case the height appears to saturate or have a maximum at $\phi = 0.834$.

Together with $\tau_{is} \sim N_{is}$ this leads to $\langle \tau_p \rangle \sim (\phi_J^{rnd} - \phi)^{-2}$. For comparison we note that the divergence of $\langle \tau_p \rangle$ in the NIB region from Fig. 5(a) for $N \approx 10^6$ and $0.800 \leqslant \phi \leqslant 0.830$ gives the similar exponent -2.1. It could thus be that this simple model captures the behavior well below jamming, but considering the bold assumptions and simplifications involved here, there is no wonder that it fails to predict the higher value of the exponent expected closer to jamming [16].

F. Analyses of C_{force}

The correlation function $C_{force}(r)$ in Eq. (4), introduced in Ref. [22], is shown in Fig. 13 for both the random and the shearing cases. We note that the magnitude of $C_{force}(r)$ for the random case is much higher than for the shearing case and that the weak signal in the latter case makes it difficult to get reliable data. Another difference is that the height (the maximum value) of the curves for the random case keeps increasing as ϕ increases, whereas, in the shearing case, the height appears to saturate, or have a maximum, at $\phi = 0.834$.

The length scale used to interpret the results in Ref. [22] is ξ_{force}, which is a measure of the distance over which the net particle forces are correlated and is determined from the

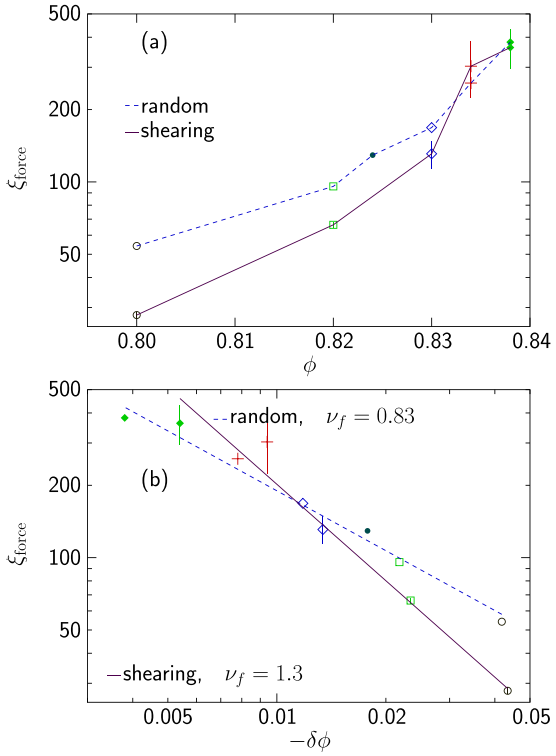

FIG. 14. The length $\xi_{\rm force}$ for the two different protocols determined from relaxations with $N \approx 10^6$. Panel (a) shows that $\xi_{\rm force}$ behaves about the same for the two different protocols but is always somewhat lower for the shearing case. Panel (b) shows attempted determinations of the critical exponent ν_f for the two cases, giving $\nu_f = 0.92$ for the random case and $\nu_f = 1.3$ for the shearing case. We consider these values to be effective exponents since they describe the behavior well away from jamming.

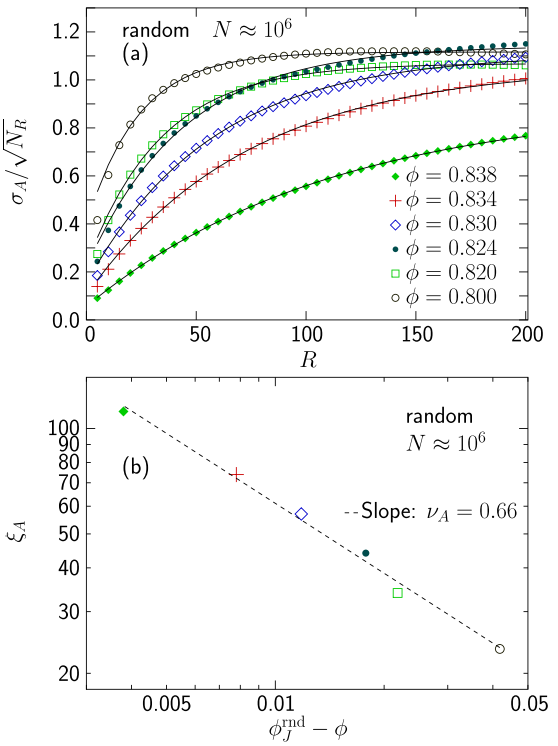

FIG. 15. Determination of a characteristic length from the density fluctuations for the random case. Panel (a) shows density fluctuations for $N = 262\,144$ and $\phi = 0.800$ through 0.838 together with lines from the fitting to Eq. (6). Panel (b) is ξ_A from these fits vs $\phi_J^{\rm rnd} - \phi$. The fit of ξ_A for $\phi \leqslant 0.830$ based on the assumption of an algebraic divergence tentatively suggests $\nu_A = 0.66$.

distance where $C_{\rm force}(r)$ turns negative. Figure 14 shows $\xi_{\rm force}$ for the two different simulation protocols. The raw data in Fig. 14(a) show that $\xi_{\rm force}$ is consistently somewhat smaller in the shearing case than in the random case, but also that this could possibly change at higher ϕ. By fitting both sets of data to algebraic divergences, $\xi_{\rm force} \sim (-\delta\phi)^{-\nu_f}$ as shown in Fig. 14(b) we find differing exponents, $\nu_f = 0.92$ for the random case and $\nu_f = 1.3$ for the shearing case. We consider these values to be only effective exponents since they are determined from $\xi_{\rm force}$ well away from jamming. (The determinations have been done with $\delta\phi = \phi - \phi_J^{\rm rnd}$, with $\phi_J^{\rm rnd} = 0.8418$ [28] for the random case, and $\delta\phi = \phi - \phi_J$, with $\phi_J = 0.8434$ [16], for the shearing case.)

It is also possible to determine a length scale in the random case from the R dependence of the density fluctuations. To that end we determine $\sigma_A(R)$ from the relaxed systems of $N \approx 10^6$ particles for $\phi = 0.800$ through 0.838 and fit data for $R \geqslant 15$ to

$$\sigma_A(R)/\sqrt{N_R} = A_0(\phi) + A_1 e^{-R/\xi_A}. \tag{6}$$

The data are shown in Fig. 15(a). The solid lines are the fitted functions. The physical interpretation of the length scale ξ_A is that the relaxation is effective only in reducing the fluctuations at length scales smaller than ξ_A. Figure 15(b) is ξ_A vs $\phi_J^{\rm rnd} - \phi$. The assumption of an algebraic divergence, $\xi_A \sim (\phi_J^{\rm rnd} - \phi)^{-\nu_A}$, with $\phi_J^{\rm rnd} = 0.8418$ [28], gives $\nu_A = 0.66$.

One could wonder whether our two different lengths, $\xi_{\rm force}$ and ξ_A, really measure the same thing but in different ways. The large difference of the exponents, $\nu_f = 0.92$ and $\nu_A = 0.66$, however, makes us conclude that that is most likely not the case, especially since the two quantities are determined from the same sets of relaxed configurations.

IV. FINITE SIZE EFFECTS IN η_p

We now leave the discussion of the relaxation time determined from relaxations of two different sets of initial configurations and instead turn to $\eta_p \equiv p/\dot\gamma$ obtained from shearing simulations. What is in focus is the claim in Ref. [22] that η_p may not be used for extracting the critical behavior, since it is plagued by strong finite size effects and is reliable only in the—presumably inaccessible—limit $L \gg \xi_{\rm force}$. We do, however, note that there is no strong numerical data in Ref. [22] in support of their claim and that our own data in Fig. 16 give no evidence for the existence of any problematic finite size effect.

Before turning to our numerical data we shortly sketch what should be expected if the jamming transition were working as an ordinary continuous transition. (We find below that it does not.) In shear-driven systems below jamming there is ample evidence for a correlation length $\xi \sim (\phi_J - \phi)^{-\nu}$,

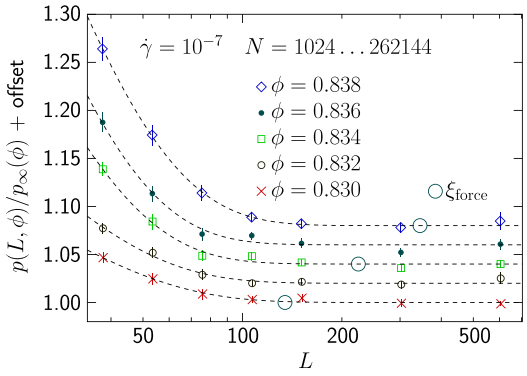

FIG. 16. Finite size dependence of p at $\phi = 0.830$ through 0.838. In contrast to the prediction in Ref. [22] that the finite size effect is governed by the rapidly increasing $\xi_{\rm force}$ (marked by big open circles on the dashed curves for $\phi = 0.830$, 0.834, and 0.838) the figure suggests an onset of finite size effects at $L \approx 100$, independent of ϕ.

with $\nu \approx 1$ [29], and it is furthermore shown that the pressure equivalent of the shear viscosity diverges as $\eta_p \sim \xi^{-\beta/\nu}$ with $\beta/\nu \approx 2.7$. For quantities such as pressure and shear stress one would then expect the introduction of a finite (small) system size L to mean that things should depend on the dimensionless quantity ξ/L, and the expectation is then that the pressure should start increasing as L decreases below some $L_c(\phi) \sim \xi$. For the density range $\phi = 0.830$ through 0.838 considered below this L_c should be expected to increase by a factor of $\approx$2.5 when the density increases from $\phi = 0.830$ to 0.838.

To examine the finite size dependence Fig. 16 we have determined $p(\phi, L)$ with shear rate $\dot\gamma = 10^{-7}$ for $\phi = 0.830$, 0.832, 0.834, 0.836, and 0.838 and $N = 1024$ through 262 144 particles, corresponding to system sizes $L \approx 37$ through $\approx$600. The data are shown in Fig. 16 as $p(\phi, L)/p_\infty(\phi)$ vs L. Since the data are normalized to unity for large L, the points for different ϕ are shifted vertically for clarity. The extrapolated $p_\infty(\phi)$ are obtained by fitting

$$p(\phi, L) = p_\infty(\phi) + C_p(\phi)e^{-L/L_c}, \tag{7}$$

shown by the dashed curves in Fig. 16.

In the figure we find evidence for a clear finite size effect setting in below a constant $L \approx 100$, for all the different densities. Likewise, from the fit to Eq. (7) we find $L_c \approx 21$ for all the densities without any trend. This is thus at odds with the expectation that p should depend on $L/\xi(\phi)$ and is difficult to reconcile with the common framework for shear-driven jamming. The invocation of logarithmic corrections to scaling—instead suggesting a scaling with $L(\ln L)^{1/4}/\xi(\phi)$ [30]—does not resolve the issue. For now we just comment that this points to the need for a novel picture of shear-driven jamming. Such work is in progress and will be presented elsewhere.

V. SUMMARY

We have performed a thorough study of the relaxation dynamics in a two-dimensional model of jamming with two different simulation protocols: relaxation of random configuration and relaxation of configurations generated through steady shearing. The question in focus has been on finite size effects and the possibility to reliably determine the critical behavior with two different methods (1) from the relation between the relaxation time, τ and the contact number deficiency, δz, and (2) from the pressure equivalent of the shear viscosity.

For the first point we first note that the identification of the NIB effect in Ref. [22], together with the claim that it works about the same for both the random case and the shearing case appears correct. Our crucial observation is, however, that there is also another finite size effect—the DF (density fluctuations) effect—which is clearly seen only for the random case and has profound consequences and adversely affects the data produced with that protocol. This then gives a rationale for trusting the analyses obtained with the shearing protocol in spite of the presence of problematic finite size effects in data obtained with the other protocol as in Fig. 1 of Ref. [22].

Another key result is that it is possible to determine the average particle relaxation time $\langle\tau_p\rangle$, which is a quantity with a well-defined thermodynamic limit, which therefore may be used to define the critical divergence, but also that τ—the energy relaxation time which has a problematic $\ln N$ dependence for very large N—may be used as a reliable estimate of $\langle\tau_p\rangle$ if one just stays clear from the very large N region of the NIB effect.

When it comes to the second point on the finite size effect on η_p, our data for $0.800 \leqslant \phi \leqslant 0.838$ give evidence for significant finite size effects for sizes below $L \approx 100$, independent of ϕ. We note first that this suggests that the data for $N = 65\,536$ and $L \approx 300$ used in scaling analyses of shear-driven jamming [16] are not too much affected by finite size effects, but also that this ϕ-independent finite size effect is at odds with the expectations from shear-driven jamming being an ordinary continuous transition.

To summarize we have examined the evidence behind the criticism of two different methods employed to determine the critical divergence of shear-driven jamming, and find that the conclusions were unnecessarily pessimistic. There do nevertheless remain many questions regarding reliable and consistent interpretations of such data as well as regarding the validity of the related theoretical approaches [15,31,32].

ACKNOWLEDGMENTS

I thank Y. Nishikawa, A. Ikeda, and L. Berthier for useful discussions and S. Teitel for many discussions as well as comments on a previous version of the article. The computations were enabled by resources provided by the Swedish National Infrastructure for Computing (SNIC), partially funded by the Swedish Research Council through Grant Agreement No. 2018-05973.

APPENDIX A: EVIDENCE FOR THIS EXTRA FINITE SIZE EFFECT FROM DATA IN REF. [22]

We here point out that the conclusion of the existence of a finite size effect other than the NIB effect, here arrived at through analyses of $H(\tau_p)$, may actually also be reached from the information presented in Ref. [22].

In Sec. III A we argued that $N = 16\,384$ at $\phi = 0.820$ is actually outside the NIB region and that the finite size dependence there therefore has to have another origin than the NIB effect. From the statement [22] that the small-N regime is a regime where "the force correlation is limited by the system size, so that $\xi_{\text{force}}(\phi, N)/L = O(1)$," together with their Fig. 5(b), which shows that $\xi_{\text{force}} \sim N^{1/2}$ at least up to $N = 128^2$, it seems that $N = 16\,384 \equiv 128^2$ at $\phi = 0.820$ is actually in this small-N regime. Furthermore, their Fig. 4(c) which shows the coarse-grained force field in a big system at the same density, $\phi = 0.820$, has structures bigger than $L \approx 150$, which is the linear size of a system with $N = 16\,384$.

Similarly, with regard to their Fig. 4(d) they write "a single correlated island seems to cover the whole system for $\phi = 0.83$, despite the fact that the system size is large $N = 262\,144$." This therefore suggests—in agreement with our Fig. 5(a)—that this point is outside the NIB region, which also implies that the N dependence at $\phi = 0.830$ in their Fig. 2(a), which shows data for $N \leqslant 262\,144$, needs an explanation other than the NIB effect.

APPENDIX B: SIZE DEPENDENCE FROM THE BINOMIAL DISTRIBUTION

For a detailed comparison of σ_A with σ_{N_R} one has to take two different factors into account. The first is the presence of two different particle sizes, and the second is the fact that for particles on the circle, only the fraction of the particles within the circle contributes to $A(R)$.

We first introduce A_c for which the particles with their centers inside R are instead included with their total area. With the areas of the big and small particles denoted by a_b and a_s, the variance in A_c gets contributions from two different sources with, on the average $N_R/2 = fN/2$ particles each, giving

$$\sigma_{A_c}^2 = \sigma_{A_c,b}^2 + \sigma_{A_c,s}^2 = \left(a_b^2 + a_s^2\right) f(1-f)\frac{N}{2} = \langle a^2 \rangle f(1-f)N, \tag{B1}$$

which gives

$$\sigma_{A_c}^2/N_R = \langle a^2 \rangle (1-f). \tag{B2}$$

Most of the deviations of $\sigma_A/\sqrt{N_R}$ from the analytically expected results in Fig. 6(a) are due to the difficulty in getting good precision in fluctuation quantities. There are, however, clear deviations from the analytical curves at small R which cannot be attributed to the limited statistics. It turns out that this is related to the way the particles that are only partly inside the region are handled. It is then only the part of the area that is inside the radius R that is counted. For small R a bigger fraction of the particles are at the boundaries, and it appears that this has the effect to reduce the fluctuations.

To compare with expressions for the variance of the density we note that the density is given by $\phi_R = A(R)/(\pi R^2)$ and that the variance of the density therefore becomes

$$\text{var}(\phi_R) = \frac{\sigma_A^2}{(\pi R^2)^2} = \frac{1}{\langle a \rangle \pi R^2}\frac{\sigma_A^2}{N_R}.$$

APPENDIX C: ONE-DIMENSIONAL MODEL

To understand the relation between N_{is} and τ_{is} we turn to a one-dimensional model with L particles with diameter equal to unity. The starting point is the zero-force configuration

$$x_i = i - (L-1)/2, \quad i = 0, \ldots, L-1,$$

which is compressed to

$$r_i = x_i + \eta_i,$$

such that the overlap between neighboring particles becomes

$$\delta_{i,i+1} = 1 - (r_{i+1} - r_i) = \eta_i - \eta_{i+1}.$$

With force $f_{i,i+1} = \epsilon \delta_{i,i+1}$ the total force on particle i, not at one of the boundaries, is

$$f_i = \epsilon\delta_{i-1,i} - \epsilon\delta_{i+1,i} = \epsilon(\eta_{i+1} - 2\eta_i + \eta_{i-1}) \approx \epsilon\Delta^2\eta,$$

and by assuming overdamped dynamics, $dr_i/dt = f_i/k_d$ one arrives at

$$\frac{\partial \eta}{\partial t} = \frac{\epsilon}{k_d}\Delta^2\eta.$$

Going to the continuum this becomes a partial differential equation

$$\frac{\partial \eta}{\partial t} = \frac{\epsilon}{k_d}\frac{\partial^2 \eta}{\partial x^2}.$$

With zero-force boundary conditions at $x = 0$ and $x = L$ the solution becomes

$$\eta(t, x) = -Ae^{-t/\tau_\eta}\sin(\pi x/L),$$

which gives the relaxation time

$$\tau_\eta = \frac{k_d}{\epsilon}\left(\frac{L}{\pi}\right)^2,$$

and by finally considering the decay of the energy, with is $\sim\delta^2$, one arrives at

$$\tau_{1\text{d}}/(k_d/\epsilon) = \frac{1}{2\pi^2}L^2 \approx 0.05L^2.$$

When the particles are instead arranged in an orderly two-dimensional array (which is of course very different from the situation in our simulations) we make use of $L = \sqrt{N}$ to get $\tau_{2\text{d}}(N)/(k_d/\epsilon) \approx 0.05N$.

[1] A. J. Liu and S. R. Nagel, Nature (London) **396**, 21 (1998).

[2] C. S. O'Hern, L. E. Silbert, A. J. Liu, and S. R. Nagel, Phys. Rev. E **68**, 011306 (2003).

[3] D. J. Durian, Phys. Rev. Lett. **75**, 4780 (1995).

[4] P. Olsson and S. Teitel, Phys. Rev. Lett. **99**, 178001 (2007).

[5] B. Andreotti, J.-L. Barrat, and C. Heussinger, Phys. Rev. Lett. **109**, 105901 (2012).

[6] T. Hatano, J. Phys. Soc. Jpn. **77**, 123002 (2008).

[7] C. Heussinger and J.-L. Barrat, Phys. Rev. Lett. **102**, 218303 (2009).
[8] T. Hatano, Phys. Rev. E **79**, 050301(R) (2009).
[9] T. Hatano, Prog. Theor. Phys. Suppl. **184**, 143 (2010).
[10] B. P. Tighe, E. Woldhuis, J. J. C. Remmers, W. van Saarloos, and M. van Hecke, Phys. Rev. Lett. **105**, 088303 (2010).
[11] T. Hatano, J. Phys.: Conf. Ser. **319**, 012011 (2011).
[12] M. Otsuki and H. Hayakawa, Phys. Rev. E **83**, 051301 (2011).
[13] E. Lerner, G. Düring, and M. Wyart, Proc. Natl. Acad. Sci. USA **109**, 4798 (2012).
[14] P. Olsson, Phys. Rev. E **91**, 062209 (2015).
[15] H. Ikeda, J. Chem. Phys. **153**, 126102 (2020).
[16] P. Olsson and S. Teitel, Phys. Rev. E **83**, 030302(R) (2011).
[17] S. H. E. Rahbari, J. Vollmer, and H. Park, Phys. Rev. E **98**, 052905 (2018).
[18] P. Olsson, Phys. Rev. Lett. **122**, 108003 (2019).
[19] M. Wyart, L. E. Silbert, S. R. Nagel, and T. A. Witten, Phys. Rev. E **72**, 051306 (2005).
[20] C. P. Goodrich, A. J. Liu, and S. R. Nagel, Phys. Rev. Lett. **109**, 095704 (2012).
[21] A. Ikeda, T. Kawasaki, L. Berthier, K. Saitoh, and T. Hatano, Phys. Rev. Lett. **124**, 058001 (2020).
[22] Y. Nishikawa, A. Ikeda, and L. Berthier, J. Stat. Phys. **182**, 37 (2021).
[23] D. J. Evans and G. P. Morriss, *Statistical Mechanics of Nonequilibrium Liquids* (Academic Press, London, 1990)
[24] D. Vågberg, P. Olsson, and S. Teitel, Phys. Rev. Lett. **112**, 208303 (2014).
[25] Y. Wu, P. Olsson, and S. Teitel, Phys. Rev. E **92**, 052206 (2015).
[26] The quantity plotted in Ref. [22] is obtained by also dividing by $2\pi r$ to compensate for the contribution of the increasing number of particles with the distance. We have made use of that expression without this division to make it easier to compare the shape of these curves.
[27] A. Donev, F. H. Stillinger, and S. Torquato, Phys. Rev. Lett. **95**, 090604 (2005).
[28] D. Vågberg, D. Valdez-Balderas, M. A. Moore, P. Olsson, and S. Teitel, Phys. Rev. E **83**, 030303(R) (2011).
[29] P. Olsson and S. Teitel, Phys. Rev. E **102**, 042906 (2020).
[30] R. Kenna, Nucl. Phys. B **691**, 292 (2004).
[31] E. DeGiuli, G. Düring, E. Lerner, and M. Wyart, Phys. Rev. E **91**, 062206 (2015).
[32] P. Olsson, Phys. Rev. E **93**, 042614 (2016).